# Dynamic Vision-Enabled Machine Condition Monitoring: A Point Cloud-Based Diagnostic Methodology

Tongmiao Xu
School of Mechanical Engineering, Xi'an Jiaotong University
Xi'an 710049, People's Republic of China
xtongmiao@gmail.com

Dehao Cai
School of Mechanical Engineering, Xi'an Jiaotong University
Xi'an 710049, People's Republic of China
cdh7654321@gmail.com

Shaojie Yang
Department of Mechanical and Aerospace Engineering at the University of California San Diego, La Jolla, CA 92093 USA
shy026@ucsd.edu

Shuai Gu
School of Management, Xi'an Jiaotong University
Xi'an 710049, People's Republic of China
2216113486@stu.xjtu.edu.cn

Xiang Li *
Key Laboratory of Education Ministry for Modern Design and Rotor-Bearing System, Xi'an Jiaotong University
Xi'an 710049, People's Republic of China
lixiang@xjtu.edu.cn

***Abstract*—Event-based cameras are an emerging type of Dynamic Vision Sensor. Unlike traditional standard cameras, they record the occurrence of brightness changes, which enables them to achieve low latency, high dynamic range, and high temporal resolution. To explore the application of contactless event data in machine fault diagnosis, this article draws inspiration from the similarity in data format between event data and 3D point cloud data. While point cloud data is widely employed in computer vision tasks, particularly in intelligent systems like autopilots and robots, its usage in industrial settings is scarce. This article presents one of the pioneering attempts in the current literature on using a 3D point cloud data algorithm to process event data for machine fault diagnosis. A geometric data structure is proposed to represent event information and a deep learning method on point cloud data is employed for classification to perform diagnosis tasks. The article conducts experiments on diagnosing rotating machine faults using event-based cameras. It has been extensively validated that utilizing point sets derived from dynamic vision data captured by event-based cameras can achieve high accuracy in fault diagnosis. Given their economic viability, installation flexibility, and data efficiency, event-based cameras emerge as a promising solution for non-contact monitoring of machine health conditions and fault diagnosis.**

***Keywords-deep learning; event-based camera; fault diagnosis; machine vision; point clouds***

## I. INTRODUCTION

Intelligent machinery fault diagnosis has reached great success with big data-driven methods in the past decades [1-7]. In the current literature, contact sensors such as accelerometers are generally used to measure vibration signals due to their high fault sensitivity[6,7]. Meanwhile, there is growing interest in non-contact sensors for their flexibility and portability in industrial applications[8,9]. Recently, contactless vibration sensors like radar-based, eddy current, and digital camera systems have been developed[10-14], each with its own performance, cost, and suitability tradeoffs. Therefore, it is necessary to find a suitable non-contact vibration sensor to establish a dataset for machine health condition monitoring and develop corresponding data processing frameworks and algorithms for fault feature extraction. Promisingly, Event-based cameras, which selectively respond to changes in pixel brightness, enable the collection of vibration signals from machines with high temporal resolution, making them hold great potential for achieving effective fault diagnosis performance [13,14].

Recently, event-based cameras have been successfully developed to address various tasks across disciplines, which are utilized to collect dynamic vision data [15]. In [16], event-based cameras were employed in self-driving vehicle situations", enabling the development of various assistance systems through the analysis of event-based machine vision data. Zhou et al. [16] introduced a vision-based navigation system that utilizes data captured by event-based cameras, demonstrating robust performance even in difficult lighting conditions, such as dim environments. In [18], Li presents the initial exploration of utilizing contactless dynamic vision data for machine fault diagnosis. The approach involves representing the data as a two-channel image-shaped representation, where the cumulative number of positive and negative events at each pixel is captured. A deep convolutional neural network (DCNN) designed for 2D data is employed for the analysis. The cumulative brightness change approach may offset some of the features related to brightness changes, whereas preserving each event independently would allow for better utilization of the unique characteristics of each point. By using relative coordinates together with brightness change features, we can capture event-to-event relations. Inspired by the similarities between event stream data and point cloud data, this article proposes the use of event-based machine vision data to construct point cloud datasets for contactless measurement of machine vibrations.

Point cloud, as an important geometric data structure, has seen advancements in analysis techniques and application domains. In [19], a novel deep neural network PointNet is

designed to directly process raw point cloud data. Building upon this, [20] introduces the PointNet ++ network, which enhances the capability of point cloud data processing through the introduction of hierarchical structures, local feature extraction, and multi-scale feature fusion. In [21], a reliable robot navigation system utilizing 3-D point cloud matching between a captured observation and a stored reference map is presented. While point cloud technology has achieved significant success, its application in machine fault diagnosis is still limited. The use of network architectures designed for point sets provides an effective method for processing event-based camera vision data, and the feasibility and effectiveness of this approach in solving fault diagnosis problems are well validated in this article.

We evaluate the proposed method on a rotating machine test rig for fault diagnosis through the dynamic vision data collected from the event-based camera, and present the following key insights:

1) A new event data processing framework is established, which incorporates fault periodicity feature extraction and fault spatial feature transformation techniques to construct the point cloud data sets.

2) An enhanced algorithm, derived from PointNet++, is specifically designed for event representations after the transformation process and is adopted for fault pattern recognition.

## II. Approach

### A. Dynamic Vision Data Representation and Transformation

In our work, we use event-based cameras to obtain dynamic vision data. An event is sent by an activated pixel when its brightness change is above a predefined threshold at a specific time. The time sequence of the recorded events constitutes the dynamic vision data in machine condition monitoring. The pixel records the current brightness value and continues to monitor for subsequent changes above the threshold using the recorded value as a reference. The event is denoted as $\boldsymbol{e} = [\boldsymbol{x}, \boldsymbol{y}, \boldsymbol{t}, \boldsymbol{p}]$ where the spatial coordinates are followed by the timestamp of the event. $p$ indicates the polarity of the brightness change, which is set to positive or negative one, signifying an increase or decrease in brightness change of the pixel. The events are denoted as $\{\boldsymbol{e_i}\}_{\boldsymbol{i=1}}^{\boldsymbol{n_e}}$ for $i = 1$ to $\boldsymbol{n_e}$, and $\boldsymbol{n_e}$ is the total number of events recorded within a specific sample ROI during the data collection period $\boldsymbol{t_{e,n}}$. Here, $n$ means the rotating speed. Specifically, $\boldsymbol{e_i} = [\boldsymbol{x_i}, \boldsymbol{y_i}, \boldsymbol{t_i}, \boldsymbol{p_i}]$.

This representation shares similarities with point cloud data. Taking the example of the data used by the PointNet algorithm, ModelNet40 consists of six dimensions, including the position of the point $(x, y, z)$ and the surface's normal vector$(N_x, N_y, N_z)$where the point is located. In the case of event data, x and y coordinates are referenced to the origin of the region of interest (ROI). In this study, the timestamp t is considered as a spatial concept, representing the z-axis. Additionally, the polarity $(p)$ serves as a feature of each point, like how a vector represents a feature in point cloud data.

To elaborate, the proposed transformation approach considers the change in event brightness polarity over time as a variation in spatial coordinates. Instead of compressing features over time to form a 2-D image type sample by accumulating the polarity values of asynchronous positive or negative events, this event-based data transformation treats asynchronous events with different z-values.

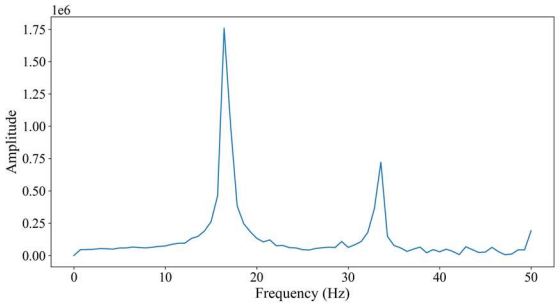

Figure 1. Event-based vibration spectrum for ball fault under 1000r/min condition

During a continuous operating period of the monitored machine, it is necessary to segment the continuous segments to obtain multiple 3D objects. The repetitiveness of fault characteristics can serve as a basis for dividing the samples, ensuring that samples with the same fault exhibit consistency and possess similar fault features.

(i)fault periodicity feature extraction

In terms of the temporal characteristics of machine failures, the brightness variations captured by the event camera exhibit periodic changes related to the rotation cycle of the machine. A notable observation is that the spectral peaks in the event-based vibration spectrum align precisely with the bearing's rotation speed and fault mechanisms. Fig. 1 illustrates the event-based bearing vibration spectrum, where these characteristic frequency peaks can be clearly identified.

Therefore, to ensure that each sample fully represents the fault properties occurring during a single rotation cycle, the data collection time $\boldsymbol{t_{e,n}}$ for each sample is set to $\frac{\boldsymbol{60}}{\boldsymbol{n}}$.

(ii)fault spatial feature transformation:

To eliminate the influence of time units, the time values are normalized in the machine condition monitoring scenario. However, to preserve the spatial characteristics of the x and y variables without altering the shape of the fault features, standardization is applied to the x and y variables. The transformation approach leverages the characteristics of point cloud data to effectively represent event data, extracting meaningful fault features for analysis. The position of the transformed point cloud data is defined as:

$$\boldsymbol{z_i^{'}} = \frac{\boldsymbol{t_i - t_{min}}}{\boldsymbol{t_{max} - t_{min}}} \tag{1}$$

$$\boldsymbol{x_i^{'}} = \frac{\boldsymbol{x_i}}{\boldsymbol{\max_{i \in n_e}} \sqrt{\boldsymbol{x_i}^2 + \boldsymbol{y_i}^2}} \tag{2}$$

$$\boldsymbol{y_i^{'}} = \frac{\boldsymbol{y_i}}{\boldsymbol{\max_{i \in n_e}} \sqrt{\boldsymbol{x_i}^2 + \boldsymbol{y_i}^2}} \tag{3}$$

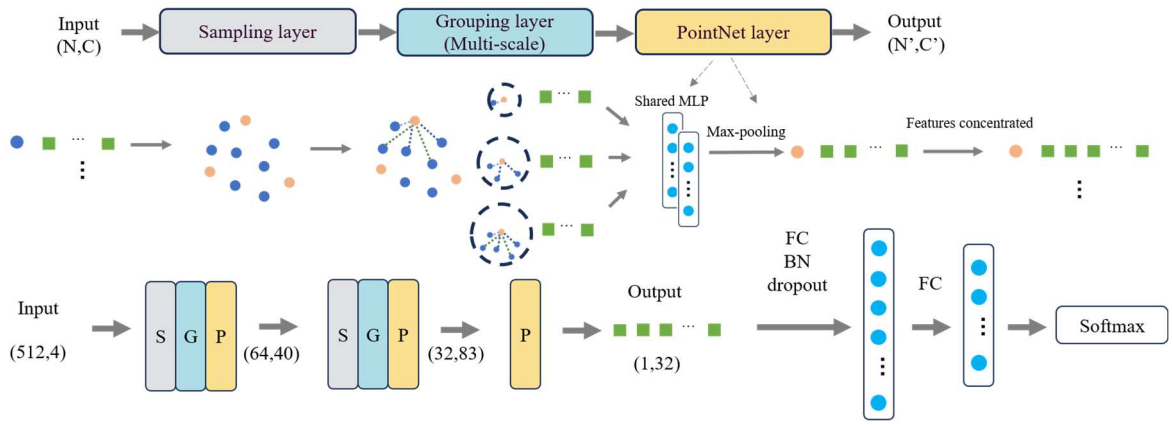


Figure 2. Complete network architecture

## B. *Network Architecture*

In this article, Fig.2 illustrates the complete network architecture, which is designed for a classification task using a four-channel event representation as input. The model is based on the foundational framework of PointNet++, with a hierarchical feature learning approach for classification.

The hierarchical feature learning approach consists of two levels of set abstraction and an additional PointNet level. Within each level, the point set feature learning process effectively captures point-to-point relations within local regions by utilizing both relative coordinates and point features.

The set abstraction level is composed of three key layers: the Sampling layer, the Grouping layer, and the PointNet layer.

Notably, the Sampling layer employs iterative farthest point sampling (FPS) to select a subset of $N'$ points from the input $N$ points to ensure representative coverage of the point set. The grouping layer incorporates multi-scale grouping (MSG) based on the PointNet++ algorithm, enabling each abstraction level to extract multiple scales of local patterns and integrate them into the global feature representation. Later, a max pooling layer is applied in the PointNet layer as a symmetric function to gather information from all the neighboring points around the centroid points. By taking the maximum value within the local region, the max pooling layer ensures the invariance of the network to the input sequence.

The set abstraction level takes an $N \times (d + C)$ matrix as input, where N represents the number of points, d represents the dimension of the coordinates, and $C$ represents the dimension of the point features. The output of the set abstraction level is an $N' \times (d + C')$ matrix, containing $N'$ subsampled points with updated features represented by $C'$. The sampling layer chooses $N'$ centroids so that the grouping layer takes as input the point set of size $N \times (d + C)$ along with the coordinates of the centroids, which are of size $N' \times d$. It produces multi-scale grouping information for these centroids, resulting in output groups of size $N' \times K_i \times (d + C_i)$, where i ranges from 1 to s. Here, Ki represents the number of points in each group, determined by the radius of the ri ball, and s represents the total number of different scales. Each scale of grouping corresponds to a different feature vector length, denoted as $C_i$.

In PointNet layer, each local region is abstracted by its centroid and a local feature that encodes information about the centroid's neighborhoods. For each of the $K_i$ points within a local region, a shared Multi-Layer Perceptron (MLP) is applied. This MLP consists of d fully connected layers with widths $\boldsymbol{l_1 l_2, \dots, l_d}$, denoted as MLP $[\boldsymbol{l_1 l_2, \dots, l_d}]$. These layers perform feature extraction on each point within the local region followed by a max pooling operation. The features extracted from multiple scales of local patterns are then combined. As a result, the output data size becomes $N' \times (d + \Sigma C_i)$, where $\sum C_i = \sum_i \boldsymbol{l_d}$

After two layers of 'S-G-P', the subsequent PointNet layer operates on the output of the previous layers. In this PointNet layer, a shared MLP is used to process all the input points N' and a max pooling operation aggregates the outputs into a single vector $1 \times \Sigma C_i$.

Finally, a fully connected layer with width $fc_1$ is applied, followed by batch normalization, Rectified Linear Unit (ReLU) activation, and dropout regularization. The dropout rate is noted as $d_p$, and it helps prevent overfitting by randomly dropping out a fraction of the neurons during training. A fully connected layer comprising $fc_2$ units is incorporated, and a softmax activation function is applied. Each neuron in this layer represents the confidence value for a different machine health condition.

## C. *Process Overview*

We consider various machine health conditions to create multiclass classification problem in our work. Fig. 3 shows the overview of the intelligent machinery fault diagnosis technique.

The event-based cameras collect of the monitored machine during its operation. Events are activated and captured under different setup environments. The raw event data undergoes the periodicity feature extraction and spatial feature transformation process to convert it into point cloud data representations, enabling further processing. To obtain samples, this study employs a method that involves randomly selecting regions of interest (ROIs) within the spatial domain of the coupler region (Fig.5). Subsequently, the classification network is set up and undergoes a training phase where it learns from the labeled point net dataset. After training, the model is evaluated on its ability to generalize to new, unseen data consists of point sets representing various fault scenarios.

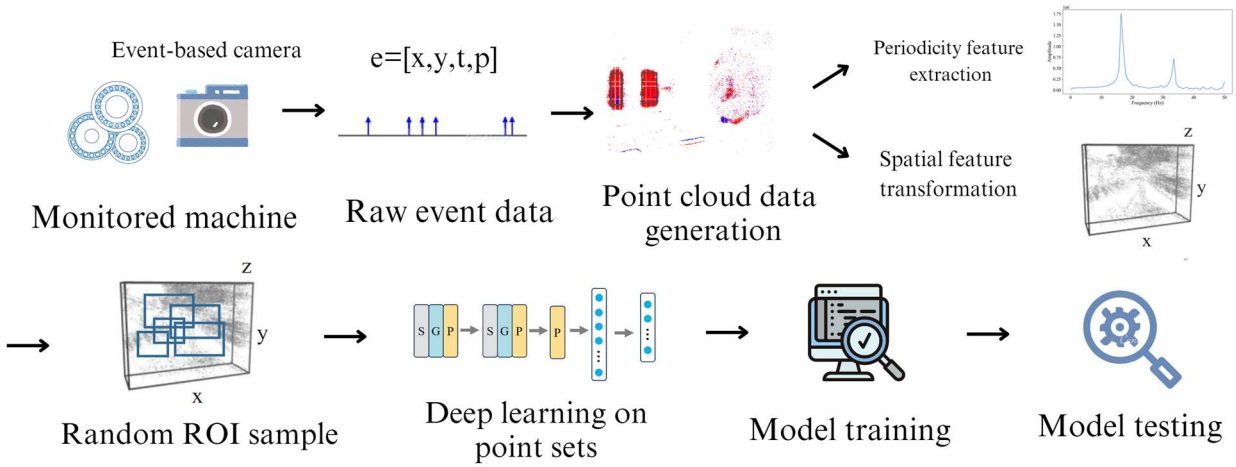


Figure 3. Overview of the intelligent machinery fault diagnosis technique

## III. EXPERIMENTS

### A. *Dynamic vision Dataset*

In this work, we assess our method to perform fault diagnosis tasks based on the dynamic vision dataset on a rotating machine. In the experimental setup, an ER-16 K bearing supporting a rotating shaft powered by an electric is used. We evaluate four distinct bearing states: healthy, inner race fault, ball fault, and outer race fault conditions. To simulate practical faults, the faults are manually introduced at different locations of the bearings using handheld tools, with depths typically around 1 mm. The experiments are conducted at two different rotating speeds: 1000 and 1500 r/min. An event-based camera is positioned at three locations relative to the bearing: in front, 45° to the left, and 45° to the right in Fig.4. This arrangement allows the camera to capture the dynamic vision data from various angles, minimizing the impact of factors like occlusions, reflections, or variations in the bearing's appearance from a single viewpoint. Consequently, measurements are obtained for four bearing health conditions under two rotating speeds, with each condition monitored from three distinct camera angles.

The event-based camera used in this study is the Gen 3.1 Prophesee event-based vision sensor. It has an effective pixel resolution of 640 × 480, a typical latency of 200 μs, and a maximum readout throughput of 50 Mevents/s. The experiments are conducted under normal light conditions in the laboratory.

Specifically, events activated in the coupler part of approximately 200×150 pixel area are selected in ROIs to examine the impact of the bearing vibration and analyzed for fault diagnosis. Bearing faults are found to have subtle influences on coupler motion, and this part exhibits a higher density of events compared to other areas of the test rig. The specific coordinate boundaries of the overall ROI vary depending on the angles of data collection, as shown in Fig.5.

To reduce the sensitivity of the analysis to the exact placement of the ROI, for each sample within the defined overall ROI, different regions of 25×25pixel size are randomly selected for different time segments of the data, as illustrated in Fig.5. For the sake of clarity, the viewpoint refers to the frontal view of the point cloud data.

This approach helps make the methodology more versatile and applicable across different camera viewing angles or experimental setups. What's more, pointsets for different health conditions captured from the position of the same angle appear similar with no noticeable differences that can be intuitively discerned. This observation indicates that the machine fault diagnosis problem based on dynamic vision is highly challenging.

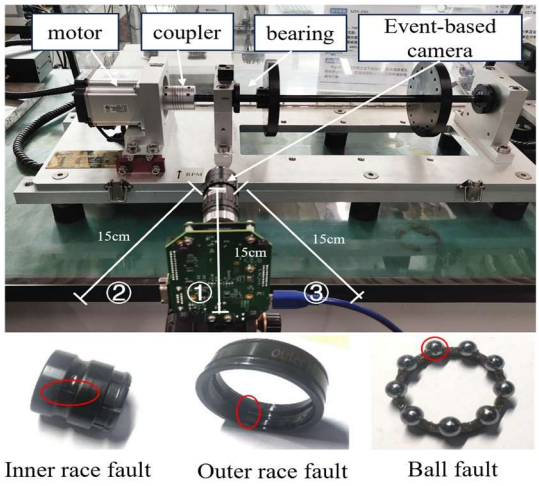


Figure 4. Experimental setup and three locations of camera

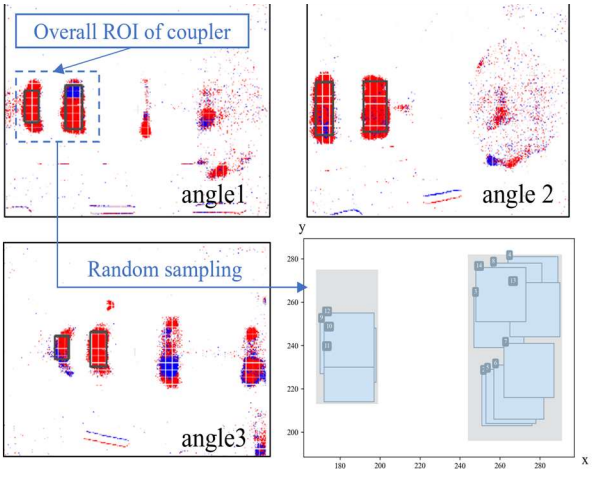


Figure 5. Examples of selection of overall ROI in monitor angles 1,2 ,3 for the bearing ball fault conditions and random sampling of ROIs

TABLE I. EVALUATION TASKS IN OUR WORK

| Task name | Camera position | Condition(r/min) | Training sample no. | Testing sample no. |
|---|---|---|---|---|
| A1 | 1 | 1000 | 560 | 56 |
| A2 | 1 | 1000<br>1500 | 1120 | 112 |
| B1 | 1,2,3 | 1000 | 1680 | 168 |
| B2 | 1,2,3 | 1000<br>1500 | 3360 | 336 |

## B. *Evaluations and Results*

Specifically, each machine health condition is represented by 140 training samples and 14 testing samples, corresponding to each rotational speed and camera position, where each sample consists of 1024 uniformly sampled points. The period of each sample is set according to the condition as described in Section II.A. Four fault diagnosis tasks are evaluated as shown in TABLE I. Tasks A1 and A2 only use data obtained from a single camera position, while tasks B1 and B2 also consider data from the other two locations. Additionally, the tasks differ in the operating conditions of the rotating speed.

The batch size is set to 16, the learning rate is set to 0.001, the number of epochs is set to 200, $n_e$ is 1024, $fc_1 1$ is 64, $fc_2$ is 32, and $d_p$ is 0.5.

Fig.6 shows the results of the tasks and indicates that the testing accuracy for the four fault diagnosis tasks is generally over 85%. Notably, tasks A2 and B2, conducted under the 1000r/min and 1500r/min rotating speeds, achieve higher accuracy compared to tasks A1 and B1. Therefore, it's validated that the point cloud data representation and the proposed transformation process can effectively extract invariant features across domains. Furthermore, it is noticed that tasks B1 and B2, which involve data from multiple camera positions, generally maintained a relatively high accuracy. This indicates that the fault diagnosis models can generalize well and perform accurately across a range of operating scenarios. These quantitative performance metrics suggest the efficacy of the dynamic vision data in solving the machine fault diagnosis classification problem.

In our research, a GeForce RTX 3090Ti GPU and an Intel i7 CPU were utilized, and the PyTorch programming framework is used. The average model training time for task B2 is 5 hours. Despite the computational demands, the results suggest that the offline nature of our work renders the computational load manageable.

Fig.7 shows the confusion matrices for task A1 and B2 to illustrate the comprehensive testing results across various machine fault categories. Consistent with the high testing accuracies reported in Fig.6, the specific fault diagnosis results are also promising. The reason task B2 achieves better fault diagnosis performance is that it utilizes more training data, including observations from different angles and positions, which enables more effective learning of the relevant fault features. The identification accuracy generally exceeds 95% for each fault mode in task B2, with a low false alarm rate. These results provide additional confirmation of the proposed method's effectiveness.

While the proposed machine vision-based approach shows promising results, there are some inherent challenges in this approach. Distinguishing the subtle variations in machinery

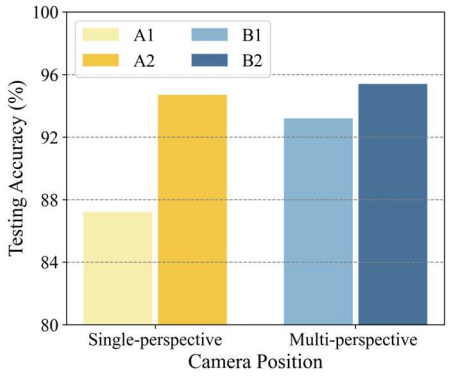


Figure 6. The testing results of the experimental performances

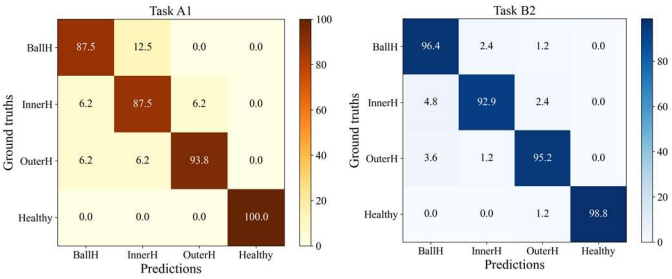


Figure 7. Confusion matrices in the fault diagnosis task A1 and B2

vibration caused by different fault modes can be challenging visually. Environmental noise and the sensor's spatial resolution also create difficulties in accurately measuring the vibration.

Despite these constraints, our work is among the first to investigate the application of event data for diagnosing machine faults. Although the visualization outcomes may not be as impressive as related studies utilizing accelerometer data, the overall findings are promising and warrant further investigation in this emerging direction of machine vision-based fault diagnosis.

# IV. CONCLUSION

This paper leverages dynamic vision data captured by event-based cameras to build a point cloud dataset and indicates that this novel type of data can be processed efficiently with our method to obtain promising results in intelligent machinery fault diagnosis.

To fully exploit the unique signatures of each event and capture intricate event-to-event relations spanning multiple scales of local patterns, this article proposes a novel geometric data structure that serves as an effective representation of event information. Subsequently, a deep learning framework is deployed on the point cloud datasets to tackle classification-based fault diagnosis tasks.

To bolster the robustness of the model, data are collected under varying rotating speeds and distinct camera angles for each fault condition. Additionally, to enhance the methodology's generalizability across diverse camera viewing angles and experimental configurations, we randomly select various regions across different temporal segments of the collected data.

Experiments are conducted on rotating machine fault diagnosis to validate the proposed approach. The findings reveal that the testing accuracy obtained by the proposed method is basically higher than 95%, even across each fault mode. These promising findings confirm the event-based cameras as a viable new contactless tool for effective machine fault diagnosis.

While the results are promising, it should be noted that machine operation in industry is often non-stationary. Variations in operating conditions can noticeably influence the dynamic vision data, potentially leading to lower model performance. Additionally, as a vision-based approach, different lighting environments can significantly impact the quality of the perceived event data, thereby affecting fault diagnosis performance. Further work will concentrate on improving the model's generalization ability across diverse operating and environmental conditions, as well as optimizing the model architecture.

## REFERENCES


[1] J. Liu, C. Zhang, and X. Jiang, “Imbalanced fault diagnosis of rolling bearing using improved MsR-GAN and feature enhancement-driven CapsNet,” Mech. Syst. Signal Process., vol. 168, 2022, Art. no. 108664.

[2] Y. Hu, R. Liu, X. Li, D. Chen, and Q. Hu, “Task-sequencing meta learning for intelligent few-shot fault diagnosis with limited data,” IEEE Trans. Ind.Informat., vol. 18, no. 6, pp. 3894–3904, Jun. 2022.

[3] H. Tang, Z. Liao, P. Chen, D. Zuo, and S. Yi, “A robust deep learning network for low-speed machinery fault diagnosis based on multi-kernel and RPCA,” IEEE/ASME Trans. Mechatronics, vol. 27, no. 3, pp. 1522–1532, Jun. 2022.

[4] X. Li, S. Yu, Y. Lei, N. Li, and B. Yang, “Dynamic vision-based machinery fault diagnosis with cross-modality feature alignment,” IEEE/CAA J. Autom. Sinica, vol. 11, no. 10, pp. 2068–2081, Oct. 2024.

[5] Li, Xiang, Wei Zhang, Xu Li, and Hongshen Hao. "Partial domain adaptation in remaining useful life prediction with incomplete target data." IEEE/ASME Transactions on Mechatronics (2023).

[6] Jin D, Han L, Hairui F, et al. MgNet: A fault diagnosis approach for multi-bearing system based on auxiliary bearing and multi-granularity information fusion[J]. Mechanical Systems and Signal Processing,2023,193.

[7] X. Yu et al., “Deep learning-based open set fault diagnosis by extreme value theory,” IEEE Trans. Ind. Informat., vol. 1, no. 1, pp. 185–196, Jan. 2022.

[8] Y. Sun, Y. Cao and P. Li, “Contactless fault diagnosis for railway point machines based on multi-scale fractional wavelet packet energy entropy and synchronous optimization strategy,” IEEE Trans. Veh. Technol., vol. 71, no. 6, pp. 5906–5914, Jun. 2022.

[9] Y. Cao, Y. Sun, G. Xie and P. Li, “A Sound-Based Fault Diagnosis Method for Railway Point Machines Based on Two-Stage Feature Selection Strategy and Ensemble Classifier,” in IEEE Transactions on Intelligent Transportation Systems, vol. 23, no. 8, pp. 12074-12083, Aug. 2022, doi: 10.1109/TITS.2021.3109632.

[10] Khadka A, Fick B, A fshar A, et al. Non-contact vibration monitoring of rotating wind turbines using a semi-autonomous UAV[J]. Mechanical Systems and Signal Processing,2020,138106446-106446.

[11] Chen, Xinrui, Xiang Li, Shupeng Yu, Yaguo Lei, Naipeng Li, and Bin Yang. "Dynamic vision enabled contactless cross-domain machine fault diagnosis with neuromorphic computing." IEEE/CAA Journal of Automatica Sinica 11, no. 3 (2024): 788-790.

[12] Guang, Ruiyi, Xiang Li, Yaguo Lei, Naipeng Li, and Bin Yang. "Non-Contact machine vibration sensing and fault diagnosis method based on event camera." In 2023 CAA Symposium on Fault Detection, Supervision and Safety for Technical Processes (SAFEPROCESS), pp. 1-5. IEEE, 2023.

[13] G. Chen, H. Cao, J. Conradt, H. Tang, F. Rohrbein, and A. Knoll, “Eventbased neuromorphic vision for autonomous driving: A paradigm shift for bio-inspired visual sensing and perception,” IEEE Signal Process. Mag., vol. 37, no. 4, pp. 34–49, Jul. 2020.

[14] B. Li et al., “Enhancing 3-D LiDAR point clouds with event-based camera,” IEEE Trans. Instrum. Meas., vol. 70, 2021, Art. no. 9511712.

[15] G. Gallego et al., “Event-based vision: A survey,” IEEE Trans. Pattern Anal. Mach. Intell., vol. 44, no. 1, pp. 154–180, Jan. 2022.

[16] G. Chen, H. Cao, J. Conradt, H. Tang, F. Rohrbein, and A. Knoll, “Eventbased neuromorphic vision for autonomous driving: A paradigm shift for bio-inspired visual sensing and perception,” IEEE Signal Process. Mag., vol. 37, no. 4, pp. 34–49, Jul. 2020.

[17] Y. Zhou, G. Gallego, X. Lu, S. Liu, and S. Shen, “Event-based motion segmentation with spatio-temporal graph cuts,” IEEE Trans. Neural Netw. Learn. Syst., early access, doi: 10.1109/TNNLS.2021.3124580.

[18] X. Li, S. Yu, Y. Lei, N. Li and B. Yang, "Intelligent Machinery Fault Diagnosis With Event-Based Camera," in IEEE Transactions on Industrial Informatics, vol. 20, no. 1, pp. 380-389, Jan. 2024, doi: 10.1109/TII.2023.3262854.

[19] Qi R C, Su H, Mo K, et al. PointNet: Deep Learning on Point Sets for 3D Classification and Segmentation.[J].CoRR,2016,abs/1612.00593

[20] Charles R Q, Li Y, Hao S, et al. PointNet++ : deep hierarchical feature learning on point sets in a metric space[C] // Advances in Neural information Processing Systems 2017, December 4-9, 2017, Long Beach, CA, USA. [S.l.: s.n.], 2017: 5099-5108.

[21] Amit E, M. J F. Robust point cloud registration for map-based autonomous robot navigation[J].EURASIP Journal on Advances in Signal Processing,2024,2024(1):